metals

MDPI

Article

Effect of Carbon Addition on Mechanical and Corrosion Properties of CoCrFeNiMn High-Entropy Alloy

Huiling Zhou [1], Hongqun Liu [2], Ji Li [1], Chengtao Li [2], Haokun Yang [3] and Yanxin Qiao [1,*]

[1] School of Materials Science and Engineering, Jiangsu University of Science and Technology, Zhenjiang 212100, China; zhouhl@just.edu.cn (H.Z.)
[2] Suzhou Nuclear Power Research Institute, Suzhou 215004, China
[3] Smart Manufacturing Division (SMD), Hong Kong Productivity Council, Hong Kong 999077, China; hkyang@hkpc.org
* Correspondence: yxqiao@just.edu.cn

Abstract

The CoCrFeNiMn High-Entropy Alloy (HEA) with 0, 0.5 and 1.0 at.% Carbon (C) addition has been evaluated by mechanical and corrosion testing, including tensile, wear and corrosion resistance testings. The result shows that the medium of 0.5 at.% C addition into HEA brings higher tensile toughness with 27,213.6 MPa%, less wear damage (0.37 mm^3) and superior thermodynamic stability (0.73 V_{SCE}), compared with that of the other two compositions. The tensile fracture observation points out that the high C addition embrittles the HEA with poorer toughness and wear resistance with content increasing to 1.0 at.%. The HEA material with 0.5 at.% C addition has high corrosion potential and the lowest corrosion current density, indicating that the appropriate C-alloying plays a significant role in determining the corrosion properties of HEA. The current study shall provide meaningful instruction for high-performance C-alloyed HEA development.

Keywords: high-entropy alloy; mechanical properties; wear; corrosion

1. Introduction

High-entropy alloy (HEA) exhibits remarkable properties of high strength, wear resistance and corrosion resistance properties when compared among the metals and alloys [1–3]. This kind of alloy is composited with five or more nominally equiatomic multi-component elements, forming a simple face-centered cubic (FCC) or body-centered (BCC) crystal structure [4–7].

To further improve the mechanical and corrosion-resistant properties of HEA, the alloying method is adopted. In the previous studies, the minor content of Al, Ti and Mo has been evaluated as an addition element of HEA [8]. The result shows that the structure of HEA changes from single-phase to dual-phase or multi-phase structures after cold work and heat treatment. In detail, Shukla et al. [9] proposed one alloyed CoCrFeNi HEA with 6.7 at.% Al, and the yield and tensile strength improved around 300 and 400 MPa, respectively. In the meanwhile, the uniform elongation improves a little. Qi et al. [10] systemically studied the addition of $(Al_{0.3}Ti_{0.2})x$ (x = 0.25, 0.5, 0.75 and 1) into the CoCrFeNi HEA system. The highest product of tensile strength and elongation to fracture was achieved with x = 0.5 of $(Al_{0.3}Ti_{0.2})x$, and the underlying strengthening mechanism came from the precipitates. More importantly, the addition of Al and Ti reduced the corrosion current density and passivation current density of the CoCrFeNi HEA with outstanding pitting corrosion resistance.

Academic Editor: Seok Su Sohn

Received: 28 November 2025
Revised: 25 December 2025
Accepted: 26 December 2025
Published: 30 December 2025

Recently, the interstitial solution elements, such as C [11,12], N [13,14] and O [15,16], play an interesting role in determining the mechanical and corrosion properties of HEA. Ye et al. [15] systemically studied the effect of N and O elements on the microstructural evolution and mechanical properties of the interstitially solutioned NbTiZrHf HEA samples. The result shows that the critical shear stress of dislocation nucleation improves in interstitial-containing NbTiZrHf HEA. In addition, Stepanov et al. pointed out that the addition of C will bring solid-solution-strengthening M_7C_3 carbides with the C content increasing, resulting in a hardness improvement of more than 70%. Ko and Hong et al. [17] analyzed the contribution of 1.84 at.% C addition in CoCrFeMnNi HEA, an improvement of 127 MPa on yield stress by C-induced friction stress associated with interstitial solution and carbide strengthening. In the meanwhile, the C addition refined the grain size and brought further grain-refinement strengthening effect. The C alloy method induces considerable scratch and wear resistance improvement accompanied with hardness [18]. Meanwhile, the previous studies of the C effect on the corrosion behavior are still in progress [19–21]. The results illustrate that the C-alloying plays a significant role in improving the corrosion resistance in chlorinated concrete solution with the content of C increasing to 0.5 at.%. Nevertheless, more C addition will deteriorate the pitting corrosion resistance and the toughness of CoCrFeMnNi HEA. The underlying mechanism has been discussed, while some details, such as the changes in fracture mechanism, wear damages and the electrochemical impedance depending on the C content are still unclear.

The present study will further reveal the Carbon-alloying effect on the fracture, wear and corrosion behavior of CoCrFeMnNi HEA, with content ranging from 0 to 1.0% at.%. As the solid-solution-strengthening mechanism plays an important role in mechanical and corrosion-resistant properties' improvement for further industrial applications. Thus, the current study systemically explores the mechanical and corrosion behaviors of HEA under various C content and points out the appropriate carbon content window for HEA design.

2. Experimental Section

The C-alloyed HEA materials were fabricated by the arc-melting method, repeated four times. The ingot was cooled in furnace, and have further annealing treatment under 1100 °C for 120 min. The detailed preparation process can be referred to our previous work [22], and the chemical composition of the casting HEAs is listed in Table 1. The changes in microstructural evolution influenced by the C addition were studied by a Rigaku SmartLab (Tokyo, Japan) 9 kW diffractometer on a Cu target using a 2θ range from 20° to 90° X-ray detection (XRD) and a Keyence VHX-7000 stereo-optical microscope (OM), respectively (Osaka, Japan).

Table 1. The chemical composition of C-alloyed HEA (at.%).

	Co	Cr	Fe	Mn	Ni	C
0 C	19.90	20.00	19.90	21.30	18.90	0.00
0.5 C	19.90	19.75	19.80	21.20	18.80	0.55
1.0 C	19.70	19.70	19.70	21.07	18.80	1.03

The tensile test was carried out under a Zwick/Roell Z250 (Ulm, Germany) with a strain rate of 0.5 mm/min, and repeated 3 times for each sample; the cross-section scale of the sample is 3.9 × 1.1 mm^2, and the gauge length is 15 mm. The counter-grinding test was performed against a GCr15 bearing steel with a loading of 500 gf, rotation of 400 rpm under 10 min, and the tested sample diameter is 3 mm. The wearing test was carried out under 20 °C and an air conditioner was adopted for temperature controlling. In the meanwhile, the fracture and wear damages were observed by an OM and an EOL

7900F scanning electron microscope (SEM, Tokyo, Japan). The electrochemical tests were performed in 3.5 wt.% NaCl solution with exposure area of 7×10 mm^2. The electrochemical measurements were carried out using a Gamry Refence 600 + electrochemical workstation (Warminster, PA, USA). A traditional three-electrode system was employed, in which the HEA sample was used as the working electrode, a platinum sheet with the surface of 10 cm^2 as the auxiliary electrode, and saturated calomel electrode (SCE) as the reference electrode. The potentiodynamic polarization measurements were scanned at a scanning rate of 0.333 mV/s. The eroded sample surface was also observed under the SEM for further study and comparison. All the electrochemical experiments were conducted at 25 ± 1 °C, and each measurement was repeated three times to ensure the accuracy of the experiments.

To further explore the corrosion mechanism of the Carbon-alloyed HEAs, the samples were immersed in a 3.5 wt.% NaCl solution for 12 h. Then, X-ray Photoelectron Spectroscopy (XPS, ESCALAB 250Xi T, Thermo Fisher Scientific, Waltham, MA, USA) testing was used to examine the properties of the passive film on the sample surface of HEA.

3. Results and Discussion

3.1. Microstructure Observation

As illustrated in Figure 1a, the XRD shows that C addition up to 1.0 at.% will not change the phase structure of the C-alloyed HEA, and only an FCC (face-centered cubic) structure is observed. Although the 1.0 C HEA shall have carbides precipitated along the grain boundary, the content and size of the carbides are too small to be detected. The OM observation of 0 C, 0.5 C and 1.0 C HEAs points out that grain size of the 0.5 C HEA (66.7 ± 24.6 mm) is larger than that of the 0 C (12.5 ± 6.9 mm) and 1.0 C (33.3 ± 11.4 mm) HEAs, as shown in Figure 1b–d. It is interesting that the 0 C HEA has a bi-model structure, where the large grains are surrounded by small grains. However, this characterization is not found in the 0.5 C and 1.0 C HEAs. In addition, the inserted SEM observation illustrates that the carbides are abundant along the grain boundary in the 1.0 C HEA. What is more, no macro-cracks were observed in all three kinds of HEA materials.

3.2. Tensile and Wear Properties

The tensile curves of the tested samples are illustrated in Figure 2a, where the yield and tensile strength of the 0 C, 0.5 C and 1.0 C HEAs are 441 ± 13 MPa and 633 ± 5 MPa, 520 ± 3 MPa and 667 ± 9 MPa, as well as 592 ± 9 MPa and 749 ± 4 MPa, respectively. To directly compare the toughness among these three samples, the product of strength and elongation (PSE) is studied. The PSE of the 0 C, 0.5 C and 1.0 C HEAs are 23,104.5 MPa%, 27,213.6 MPa% and 19,324.2 MPa%, respectively. It reveals that the 0.5 C HEA has remarkable toughness compared with the other two samples. Furthermore, the ratios of tensile strength to yield strength of 0 C, 0.5 C and 1.0 C are 1.43, 1.28 and 1.26, indicating that all three kinds of HEA has remarkable work-hardening capacities. Thus, the solid-solution- and carbide-strengthening mechanisms work in C-alloyed HEA, leading to higher tensile strength in C-alloyed HEAs. However, the plastic ductility attributed to carbides weakens in 1.0 C HEAs, where the plastic elongations of 0 C, 0.5 C and 1.0 C HEAs are $36.5 \pm 4\%$, $40.8 \pm 2\%$ and $25.8 \pm 6\%$ [23,24]. The fracture observation under SEM is exhibited in Figure 2b–d. It is found that the dimples of the 0 C HEA are much larger and deeper than those of the 0.5 C and 1.0 C HEAs, corresponding with the stronger work-hardening capacity of the 0 C HEA verified by the tensile test. With the C content increasing, the dimples of the 1.0 C HEA become much smaller and shallower than those of the 0 C and 0.5 C HEAs. The deteriorated ductility results from the carbides, along the grain boundaries [25]. This is because the limited ductility restricts the growth and coalescence of dimples, and the high distribution density of carbides disperses the nucleation of dimples [26,27].

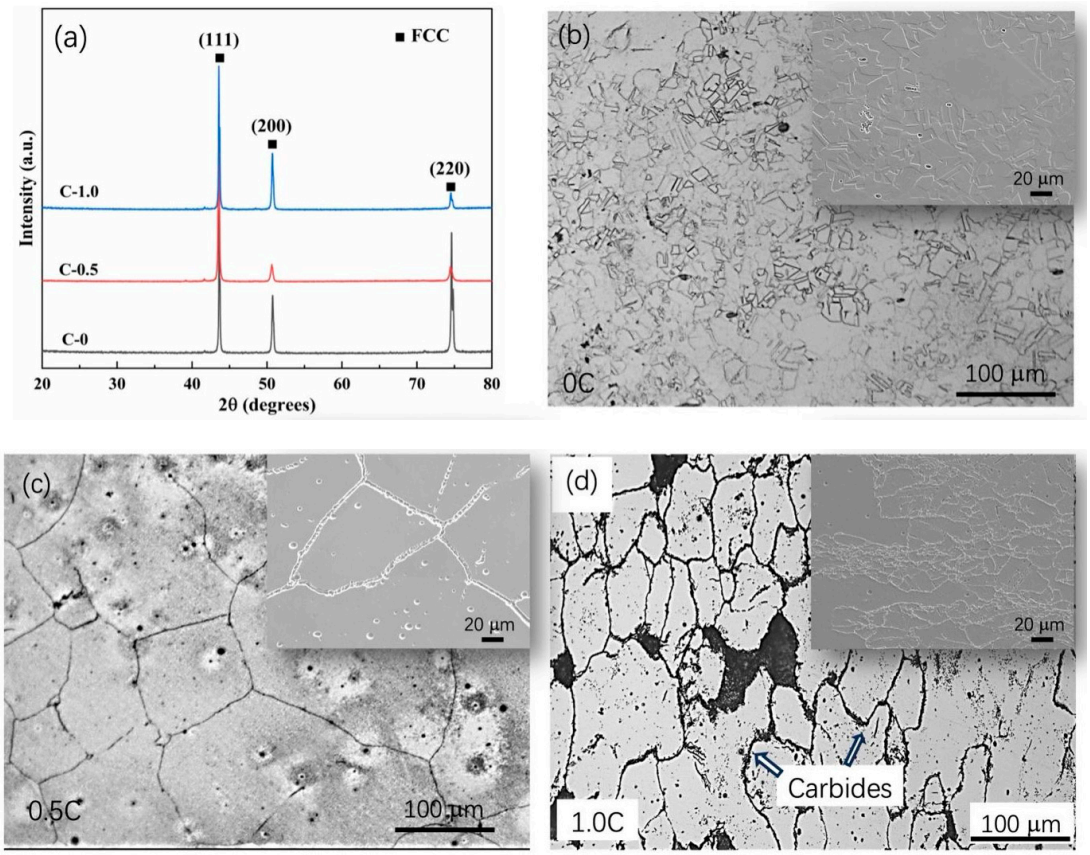

Figure 1. (**a**) XRD of C-alloyed HEA, and (**b**–**d**) OM observation of 0 C, 0.5 C and 1.0 C HEAs with detailed SEM observation inserted.

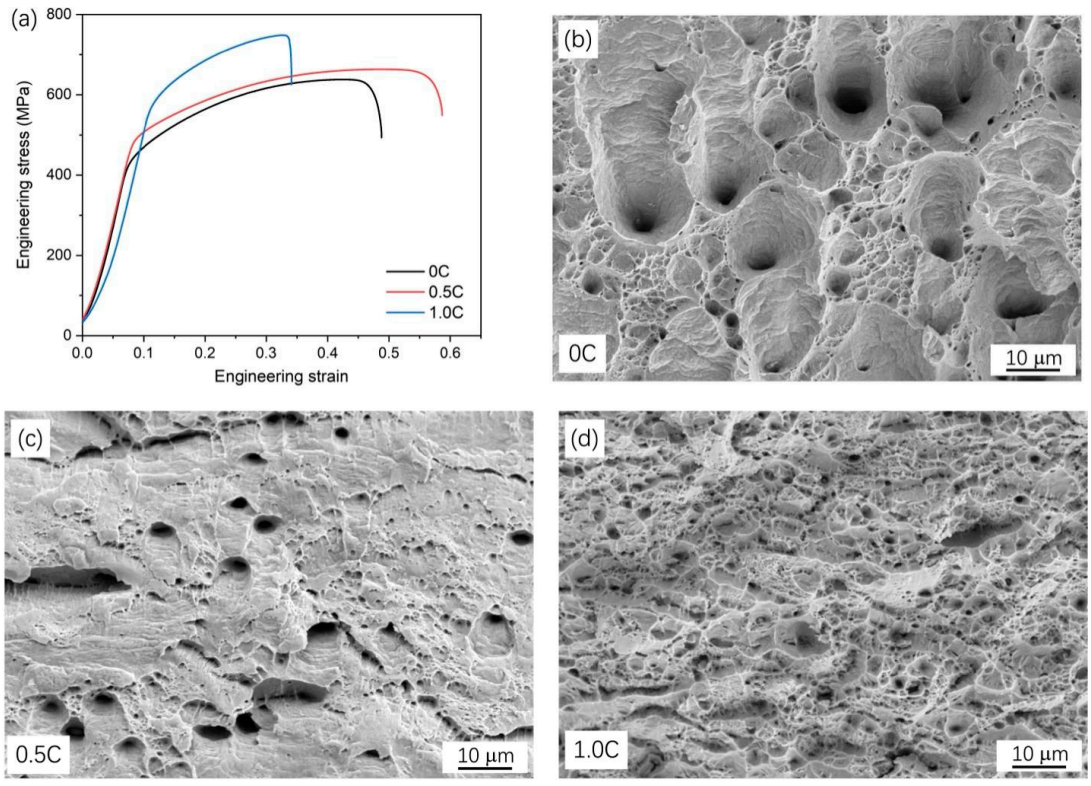

Figure 2. (**a**) The tensile curves of the tested HEA samples, and (**b**–**d**) the fracture observation of 0 C, 0.5 C and 1.0 C HEAs under SEM. (**b**) 0 C; (**c**) 0.5 C; (**d**) 1.0 C.

The morphology of the wear damages is displayed in Figure 3, where the wear volumes of the 0 C, 0.5 C and 1.0 C HEAs are 0.44 mm^3, 0.37 mm^3, and 0.40 mm^3, respectively. In addition, according to the profile of the wear pit, the 0.5 C HEA has slight wear damages. These experiment results support that the C addition shall improve the resistance to wear damages, attributing to solid-solution- and carbide-strengthening mechanisms [28]. Furthermore, taking into consideration the PSE results, the 0.5 C HEA samples exhibit the balance of strength and ductility which achieves the lowest wear damages.

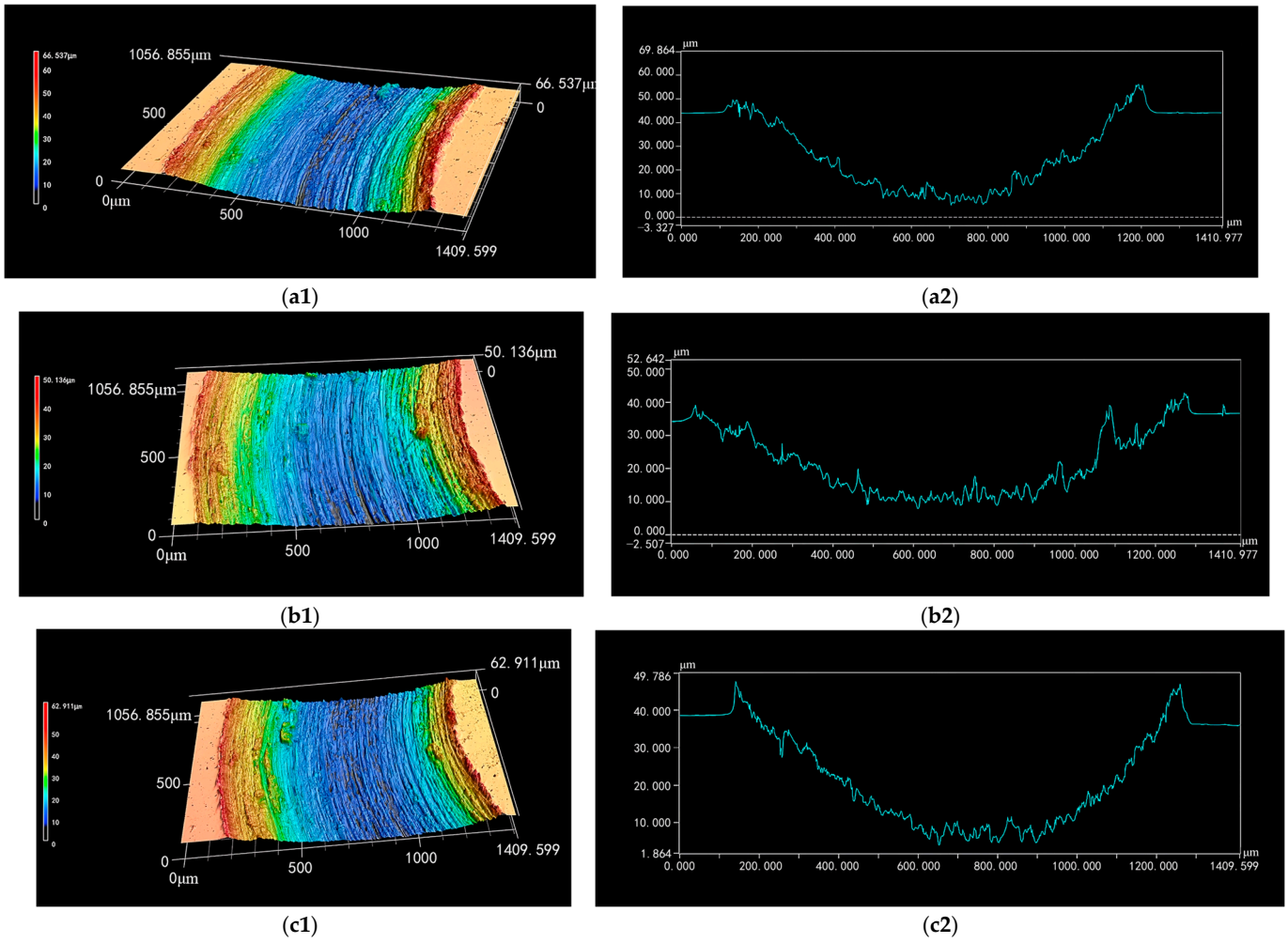

Figure 3. The morphology and profile of worn trace in (**a1**,**a2**) 0 C, (**b1**,**b2**) 0.5 C and (**c1**,**c2**) 1.0 C HEAs.

3.3. Corrosion Resistance

The potentiodynamic polarization curve of tested HEAs in 3.5 wt.% NaCl solution is shown in Figure 4a, where the corrosion potentials of the 0 C, 0.5 C and 1.0 C HEAs are −0.343 V_{SCE}, −0.262 V_{SCE}, and −0.287 V_{SCE}, and the corrosion current densities are 7.34×10^{-7} A/cm^2, 2.19×10^{-5} A/cm^2 and 3.31×10^{-5} A/cm^2, respectively. The current results illustrate that the 0.5 C HEA has the highest corrosion resistance in NaCl solution, but the corrosion current density, i.e., corrosion rate, of 0.5 C is also the lowest in these investigated materials, as shown in Table 2. Luo et al. [20] reported a similar result—that the CoCrFeMnNi HEA with a 0.5 at.% C addition has the better corrosion resistance among the C-alloyed HEAs (C at.% between 0 and 0.8). The underlying mechanism shall be attributed to the enrichment of Cr and Co elements in the passive film. Nevertheless, the further increment of C-alloying in HEAs will promote the formation of Cr- and Co-rich carbides, leading to the depletion of Cr and Co elements within passive film [21]. To reveal the corrosion characteristics, the SEM observation of the corroded samples is illustrated in

Figure 4b–d, where the depth and area of corrosion pits in the 0.5 C HEAs are much lower compared with that of the 0 C and 1.0 C HEAs. Furthermore, the density of corrosion pits in the 0.5 C HEA is lower than that of the others, corresponding with the higher corrosion current density [7,29,30].

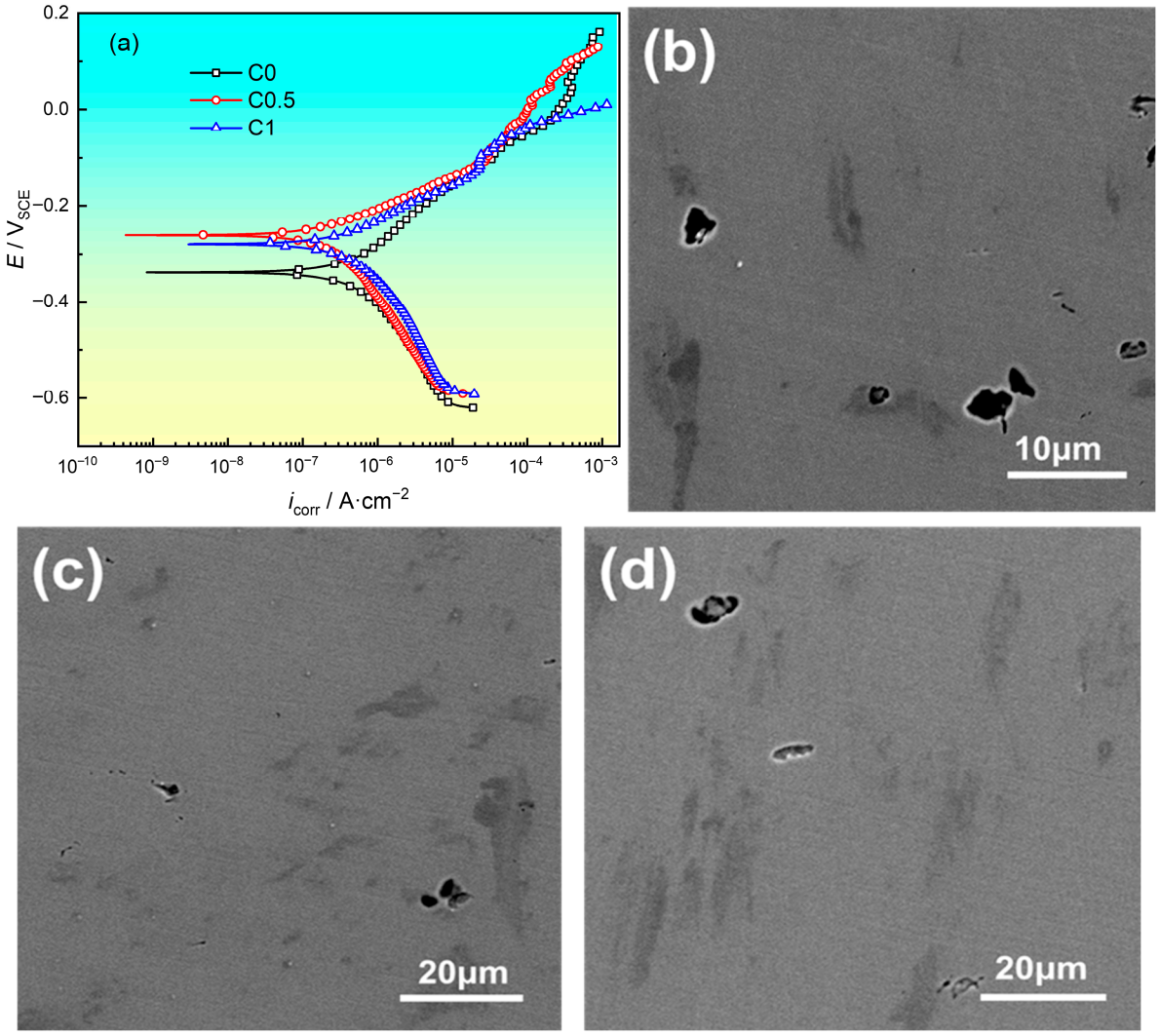

Figure 4. (**a**) The polarization curve of the tested HEA samples, and (**b**–**d**) the observation of corroded 0 C, 0.5 C and 1.0 C HEAs.

Table 2. E_{corr} and i_{corr} of the three HEAs in 3.5% NaCl solution.

	C0	C0.5	C1
E_{corr}/mV$_{SCE}$	−343.22	−264.57	−284.76
i_{corr}/A·cm^{-2}	7.34×10^{-7}	2.19×10^{-7}	3.31×10^{-7}

Furthermore, Figure 5 shows the XPS fitting results of O1s, Co 2p3/2, Cr 2p3/2, Fe 2p3/2, Mn 2p3/2, and Ni 2p3/2 of the CoCrFeMnNiC$_x$ HEA passivation film after immersion in 0.5 mol/L NaCl solution for 12 h. Co2p3/2 is composed of metallic Co (Co^0, 777.91 eV) peak, CoO (780.18 eV) peak, and Co(OH)$_2$ (782.17 eV). From the peak intensity of each cobalt component, it can be seen that the Co element of the three alloys mainly exists as Co^0. Cr 2p3/2 can be decomposed into three component peaks: metallic Cr (Cr^0, 574.6 eV), Cr_2O_3 (576.6 eV) and Cr(OH)$_3$ (578.1 eV). It can also be determined that the main forms of Cr in the passivation film are Cr and Cr_2O_3. A large number of studies have shown that the

Cr_2O_3 component is very beneficial for forming a dense and stable passivation film on the alloy surface [29,31,32]. The present study divides Fe 2p3/2 into four component peaks, i.e., metallic Fe (Fe^0, 707.9 eV), Fe_{ox}^{2+} (709.3 eV), Fe_{ox}^{3+} (710.7 eV) and Fe_{hy}^{3+} (712.7 eV). Ni $2p^{3/2}$ mainly exists in the form of metallic Ni (Ni^0, 852.3 eV). Ni is not easily oxidized and exists at the interface between the passivation film and the alloy. The metallic Ni layer can hinder the movement of ions, thereby improving the corrosion resistance of the alloy. The percentages of Co 2p3/2, Cr 2p3/2, Fe 2p3/2, Mn 2p3/2 and Ni 2p3/2 peaks of the surface passivation film formed after the 0 C, 0.5 C and 1.0 C HEAs were immersed in 3.5% NaCl solution for 12 h are marked in Figure 5. The ratio of $Cr_2O_3/(Cr + Cr(OH)_3)$ first increases and then decreases with the increase in C content, indicating that the passivation film has stronger protection for the substrate at the 0.5 C HEA [33].

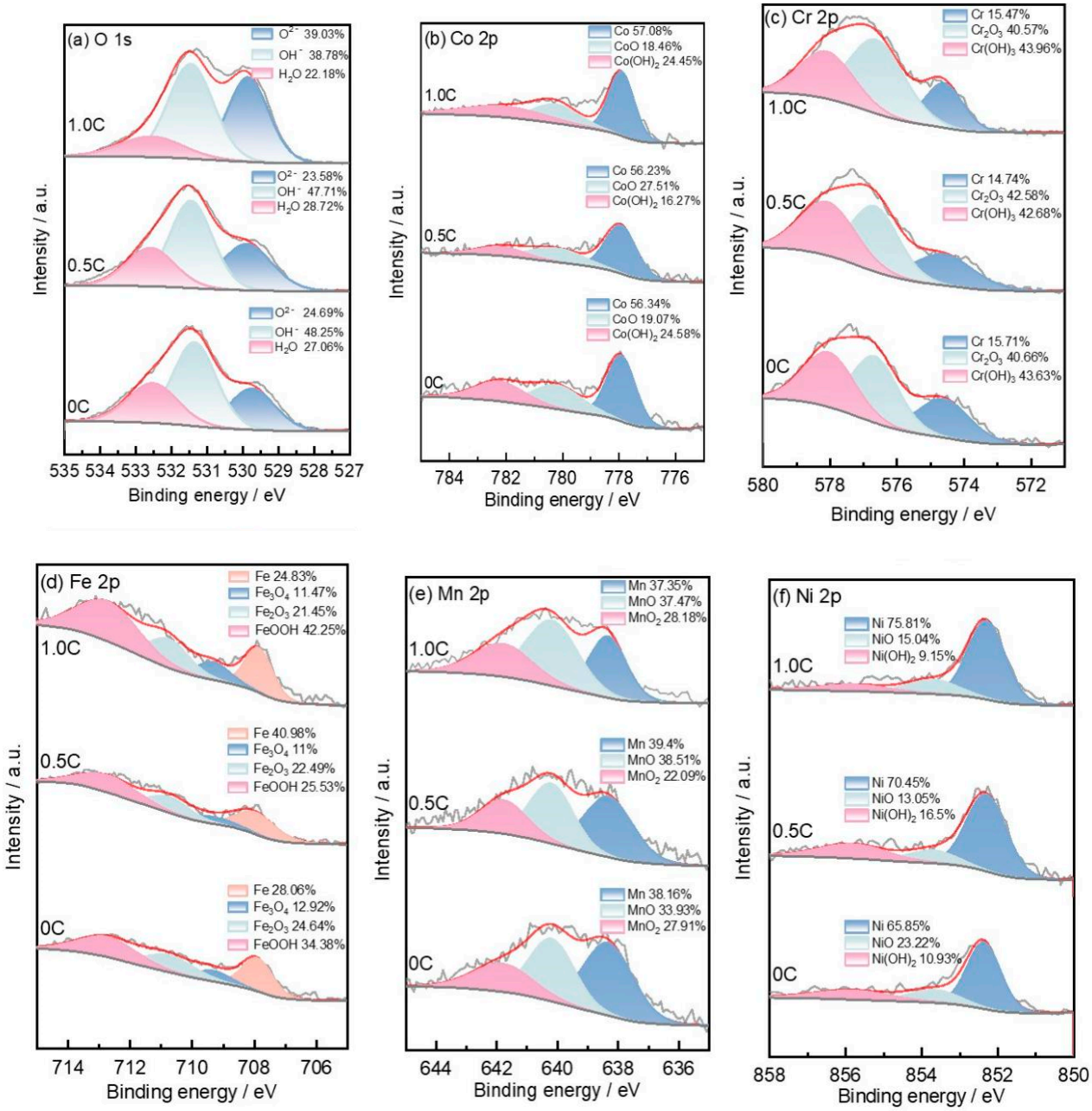

Figure 5. XPS spectra of HEA after immersion in 3.5 wt.% NaCl solution for 12h: (**a**) O1s; (**b**) Co 2p3/2; (**c**) Cr 2p3/2; (**d**) Fe 2p3/2; (**e**) Mn 2p3/2; (**f**) Ni 2p3/2. The red line in the figure is the line using to calculated the fraction of each component, the gray line is the obtained curves.

4. Conclusions

The influences of C addition on the microstructural evolution, mechanical properties, and corrosion resistance of CoCrFeNiMn HEA are discussed in the current study. The results illustrate that C has an obvious improvement in the yield with PSE of 27,213.6 MPa% and tensile strength, while sacrificing the plasticity due to the carbides. In addition, with the balance of strength and plasticity, the 0.5 C HEA exhibits better wear resistance of 0.37 mm^3. In the meanwhile, the 0.5 C HEA exhibits better thermodynamic stability in a 3.5 wt. % NaCl solution with the lowest corrosion potential of 2.19×10^{-7} A/cm^2. This is due to the ratio of $Cr_2O_3/(Cr + Cr(OH)_3)$ being the highest in the 0.5 C HEA, exhibiting stronger protectiveness on the substrate. In future studies, the other alloying candidates and the precision settings of temperature, time and atmosphere under heat treatment will be further considered to optimize the mechanical properties of HEAs. In the meanwhile, application-specific tests, such as fatigue, creep and stress-corrosion cracking testing will be carried out the performance of HEAs with designed alloying and heat treatment.

Author Contributions: Conceptualization, H.Z., H.L. and H.Y.; Methodology, J.L. and C.L.; Investigation, H.Z., J.L. and H.L.; Writing—Original Draft Preparation, H.Z., C.L., H.Y. and Y.Q.; Writing—Review and Editing, C.L., H.Y. and Y.Q.; Supervision, Y.Q.; Funding Acquisition, H.Z. All authors have read and agreed to the published version of the manuscript.

Funding: This research was funded by the National Natural Science Foundation of China (No. U25A20201).

Data Availability Statement: The original contributions presented in this study are included in the article. Further inquiries can be directed to the corresponding authors.

Conflicts of Interest: Authors Hongqun Liu and Chengtao Li were employed by the Suzhou Nuclear Power Research Institute. Author Haokun Yang was employed by the Hong Kong Productivity Council. The remaining authors declare that the research was conducted in the absence of any commercial or financial relationships that could be construed as a potential conflict of interest.

References

1. Gludovatz, B.; Hohenwarter, A.; Catoor, D.; Chang, E.H.; George, E.P.; Ritchie, R.O. A fracture-resistant high-entropy alloy for cryogenic applications. *Science* **2014**, *345*, 1153–1158. [CrossRef]
2. Zhou, Y.K.; Kang, J.J.; Jin, G.; Cui, X.F.; Zhang, J.; Ma, G.Z.; Fu, Z.Q.; Zhu, L.N.; She, D.S.; Yang, Y.Y. Effect of vacuum heat treatment on microstructure and corrosion behavior of HVOF sprayed AlCoCrFeNiCu high entropy alloy coatings. *J. Iron Steel Res. Int.* **2023**, *30*, 1550–1561. [CrossRef]
3. Luo, W.D.; Hou, T.P.; Liang, X.; Zhang, D.; Lin, H.F.; Li, Y.; Zhao, T.L.; Hu, C.Y.; Yershov, S.; Wu, K.M. Electronic-scale assessment of high-temperature oxidation mechanisms in a novel Fe-based alloy. *J. Iron Steel Res. Int.* **2024**, *31*, 982–997. [CrossRef]
4. Ma, E. Unusual dislocation behavior in high-entropy alloys. *Scripta Mater.* **2020**, *181*, 127–133. [CrossRef]
5. Nie, S.J.; Yi, X.N.; Zhou, H.L.; Zhu, H.J.; Yang, L.L.; Fu, F.L.; Li, J.Y.; Yang, H.K.; Xu, G.X.; Lu, S.; et al. Corrosion behavior of as-cast $Al_{0.75}CoFeCr_{1.25}Ni$ high entropy alloy in 0.5 mol/L NaOH solution. *J. Iron Steel Res. Int.* **2024**, *31*, 2852–2863. [CrossRef]
6. Wang, W.R.; Qi, W.; Zhang, X.L.; Yang, X.; Xie, L.; Li, D.Y.; Xiang, Y.H. Superior corrosion resistance-dependent laser energy density in $(CoCrFeNi)_{95}Nb_5$ high entropy alloy coating fabricated by laser cladding. *Int. J. Miner. Metall. Mater.* **2021**, *28*, 888–897. [CrossRef]
7. Wang, Z.; Duan, J.F.; Qiao, J.W.; Che, H.Y.; He, X.K. Influence of pH value on corrosion behavior of non-equiatomic $Fe_{40}Mn_{20}Cr_{20}Ni_{20}$ high-entropy alloy. *J. Iron Steel Res. Int.* **2025**, *32*, 1114–1124. [CrossRef]
8. Sathiyamoorthi, P.; Kim, H.S. High-entropy alloys with heterogeneous microstructure: Processing and mechanical properties. *Prog. Mater. Sci.* **2022**, *123*, 100709. [CrossRef]
9. Shukla, S.; Choudhuri, D.; Wang, T.; Liu, K.; Wheeler, R.; Williams, S.; Gwalani, B.; Mishra, R.S. Hierarchical features infused heterogeneous grain structure for extraordinary strength-ductility synergy. *Mater. Res. Lett.* **2018**, *6*, 676–682. [CrossRef]
10. Qi, W.; Wang, W.R.; Yang, X.; Zhang, G.N.; Ye, W.; Su, Y.T.; Li, Y.; Chen, S.Y. Effects of Al and Ti co-doping on the strength-ductility-corrosion resistance of CoCrFeNi-AlTi high-entropy alloys. *J. Alloys Compd.* **2022**, *925*, 166751. [CrossRef]
11. Luo, H.; Li, Z.M.; Lu, W.J.; Ponge, D.; Raabe, D. Hydrogen embrittlement of an interstitial equimolar high-entropy alloy. *Corros. Sci.* **2018**, *136*, 403–408. [CrossRef]

12. Sun, J.L.; Li, X.; Zhao, L.; Zhao, J. Effects of high-entropy alloy binders on the microstructure and mechanical/thermal properties of cemented carbides. *Int. J. Miner. Metall. Mater.* **2025**, *32*, 1190–1197. [CrossRef]
13. Klimova, M.; Shaysultanov, D.; Semenyuk, A.; Zherebtsov, S.; Salishchev, G.; Stepanov, N. Effect of nitrogen on mechanical properties of CoCrFeMnNi high entropy alloy at room and cryogenic temperatures. *J. Alloys Compd.* **2020**, *849*, 156633. [CrossRef]
14. Cui, P.P.; Li, W.; Liu, P.; Zhang, K.; Ma, F.C.; Chen, X.H.; Feng, R.; Liaw, P.K. Effects of nitrogen content on microstructures and mechanical properties of (AlCrTiZrHf)N high-entropy alloy nitride films. *J. Alloys Compd.* **2020**, *834*, 155063. [CrossRef]
15. Lei, Z.F.; Liu, X.J.; Wu, Y.; Wang, H.; Jiang, S.H.; Wang, S.D.; Hui, X.D.; Wu, Y.D.; Gault, B.; Kontis, P.; et al. Enhanced strength and ductility in a high-entropy alloy via ordered oxygen complexes. *Nature* **2019**, *565*, 546–550. [CrossRef]
16. Song, Q.N.; Tong, Y.; Li, H.L.; Xu, N.; Xu, C.B.; Bao, Y.F.; Yin, L.; Qiao, Y.X. Friction stir processing of a cast manganese-aluminum bronze for improving corrosion and cavitation erosion resistances. *Surf. Topogr. Metrol. Prop.* **2020**, *8*, 025020. [CrossRef]
17. Ko, J.Y.; Hong, S.I. Microstructural evolution and mechanical performance of carbon-containing CoCrFeMnNi-C high entropy alloys. *J. Alloys Compd.* **2018**, *743*, 115–125. [CrossRef]
18. Xiao, J.K.; Tan, H.; Chen, J.; Martini, A.; Zhang, C. Effect of carbon content on microstructure, hardness and wear resistance of $CoCrFeMnNiC_x$ high-entropy alloys. *J. Alloys Compd.* **2020**, *847*, 156533. [CrossRef]
19. Tang, Z.; Huang, L.; He, W.; Liaw, P.K. Alloying and processing effects on the aqueous corrosion behavior of high-entropy alloys. *Entropy* **2014**, *16*, 895–911. [CrossRef]
20. Luo, H.; Zou, S.W.; Chen, Y.H.; Li, Z.M.; Du, C.W.; Li, X.G. Influence of carbon on the corrosion behaviour of interstitial equiatomic CoCrFeMnNi high-entropy alloys in a chlorinated concrete solution. *Corros. Sci.* **2020**, *163*, 108287. [CrossRef]
21. Chmielak, L.; Mujica, R.L.; Niederhofer, P.; Weber, S.; Theisen, T. CrMnFeCoNi high entropy alloys with carbon and nitrogen: Mechanical properties, wear and corrosion resistance. *SN Appl. Sci.* **2021**, *3*, 835. [CrossRef]
22. Leng, C.; Yang, H.; Yi, G.; Lo, H.; Li, J.; Li, Y. The effect of carbon addition on the mechanical properties and fracture behaviors of cobalt-chromium-iron-manganese-nickel high entropy alloy. *Materialwiss. Werkst.* **2024**, *55*, 7–12. [CrossRef]
23. Chen, L.B.; Wei, R.; Tang, K.; Zhang, J.; Jiang, F.; He, L.; Sun, J. Heavy carbon alloyed FCC-structured high entropy alloy with excellent combination of strength and ductility. *Mater. Sci. Eng. A* **2018**, *716*, 150–156. [CrossRef]
24. Li, X.L.; Hao, X.X.; Jin, C.; Wang, Q.; Deng, X.; Wang, H.; Wang, Z. The determining role of carbon addition on mechanical performance of a non-equiatomic high-entropy alloy. *J. Mater. Sci. Technol.* **2022**, *110*, 167–177. [CrossRef]
25. Shen, Y.Z.; Zhang, X.B.; Wu, Y.; Xu, Z.Y.; Long, J.C. Enhanced mechanical properties of tantalum alloys via multi-principal elements and compositionally complex carbides. *J. Iron Steel Res. Int.* **2025**, *32*, 4485–4497. [CrossRef]
26. Sun, J. Effect of stress triaxiality on micro-mechanisms of void coalesence and micro-fracture ductility of materials. *Eng. Fract. Mech.* **1991**, *39*, 799–805. [CrossRef]
27. Xia, C.Q.; Hu, H.M.; Zhang, X.; Jing, R.; Liu, S.G.; Chen, B.H.; Liu, N.; Yang, T.; Li, Q. Microstructural evolution, mechanical properties, and corrosion behavior of hot-rolled Ti-Zr-Al-Sn alloys. *J. Iron Steel Res. Int.* **2025**, *32*, 4454–4471. [CrossRef]
28. Xin, B.B.; Zhang, A.J.; Han, J.S.; Meng, J. The tribological properties of carbon doped $Al_{0.2}Co_{1.5}CrFeNi_{1.5}Ti_{0.5}$ high entropy alloys. *Wear* **2021**, 484–485, 204045. [CrossRef]
29. Liu, Y.C.; Zheng, Z.B.; Xu, L.L.; Xu, Z.B.; Yin, F.X.; Zheng, K.H. Unraveling the interfacial structure of TA2 titanium-A36 steel composite plate and its corrosion behavior in marine environment. *Corros. Sci.* **2024**, *230*, 111923. [CrossRef]
30. Zhang, X.Q.; Qiang, S.H.; Fan, J.X.; Zhou, H.L.; Yang, L.L.; Tang, Y.B.; Liu, Z.H.; Lu, D.H. Annealing treatment on corrosion resistance deterioration of LPBF 316L SS in 0.1 mol/L HCl solution. *J. Iron Steel Res. Int.* **2025**, *32*, 1286–1301. [CrossRef]
31. Qiao, Y.X.; Wang, X.Y.; Yang, L.L.; Wang, X.; Chen, J.; Wang, Z.B.; Zhou, H.L.; Zou, J.S.; Wang, F.H. Effect of aging treatment on microstructure and corrosion behavior of a Fe-18Cr-15Mn-0.66N stainless steel. *J. Mater. Sci. Technol.* **2022**, *107*, 197–206. [CrossRef]
32. Zhu, H.J.; Han, J.Y.; Fang, K.W.; Zheng, Z.B.; Zhou, H.L.; Yang, L.L.; Qiao, Y.X.; Chen, J.; Cui, J.; Wang, Q. Corrosion behavior of $CoCrCu_{0.1}FeMoNi$ high entropy alloy in 0.5 mol/L NaOH solution. *J. Iron Steel Res. Int.* **2025**, *32*, 1163–1175. [CrossRef]
33. Zhu, Y.S.; Yu, S.J.; Chen, S.; Hu, B.W.; Wang, C.M.; Xu, Y.Z.; Huang, Y.; Wang, M.Y. Electrochemical behavior of $FeCoNiAl_{0.75}Cr_{1.25}$ high-entropy alloy in Na_2SO_4 solution with acidic pH. *J. Iron Steel Res. Int.* **2025**, *32*, 1151–1162. [CrossRef]